12th IFAC International Symposium on
Advanced Control of Chemical Processes
July 14-17, 2024. Toronto, Canada

Nonlinear Model Predictive Control of a Particulate Polysilicon Reactor System for Enhanced Solar Cell Production

Carlos Veloz and **Davood B. Pourkargar** ⋆

Tim Taylor Department of Chemical Engineering
Kansas State University, Manhattan, KS 66506 USA

Abstract: A predictive modeling framework for silicon production in fluidized bed reactors is proposed to characterize the particle size distribution of the product and the powder loss. Two different flow regime modeling approaches are considered to describe the silane pyrolysis reaction and characterize the deposition rate that contributes to particle growth. A discrete population balance equation is used to estimate the particle size distribution as a function of the deposition rate. A nonlinear model predictive control is then utilized to regulate the system at the desired operating conditions. Detailed open-loop and closed-loop simulation studies demonstrate the successful integration of nonlinear MPC and the proposed predictive modeling approach.

Keywords: Control of particulate processes, nonlinear process control, model predictive and optimization-based control, industrial applications of process control, process modeling and identification

1. INTRODUCTION

High-purity polysilicon, or solar-grade silicon, is a critical material in the photovoltaic supply chain, constituting approximately 20% of the total solar cell production cost. Consequently, there is a significant drive to minimize the production costs associated with solar-grade feedstock (Du et al. (2014)). Utilizing silane pyrolysis in a fluidized bed reactor (FBR) offers a promising avenue to achieve this goal, compared to the conventional Siemens process. FBR systems exhibit higher operational efficiencies and lower energy consumption, making them a more efficient platform for solar-grade silicon production. The fluidized reactor's performance has been extensively evaluated and fine-tuned for the efficient production of solar-grade silicon (Cadoret et al. (2007); Tejero-Ezpeleta et al. (2004)). Polysilicon FBR dynamics are characterized by the production scale, growth rate, and decay of the discrete particles in a continuous phase.

A particulate process involves properties distributed in both external (space and time) and internal (particle size) coordinates (Ramkrishna (2000)). The population balance equation (PBE) governs the evolution of these properties along the external coordinates. However, combining it with the mass balance equation of the continuous phase results in a set of partial integro-differential equations that are challenging to solve. Several numerical methods have been developed for solving this set of equations, with moment transformation and discretization commonly employed approaches. In particular, White et al. (2006) proposed a particulate phase model by combining the mass and population balance over discrete intervals, showing reduced computational time compared to existing methods.

⋆ Corresponding Author, Email: dbpourkargar@ksu.edu, Tel: +1 (785) 532-5584, Fax: +1 (785) 532-7372.

The challenges associated with controlling the FBR system originate from the intricate nature of gas-solid interactions. Previous research has tackled these obstacles, proposing various model-based approaches. Lai et al. (1986) introduced two models for silane pyrolysis in fluidized bed systems: one employing an ideal well-mixed reactor (CSTR) to capture the FBR system's behavior under specific conditions, and the other based on Kunii and Levenspiel (1968) more comprehensive fluidized-bubbling bed model, which better encapsulates the system's physics. Caussat et al. (1995) compared model predictions for silane pyrolysis in FBR systems against experimental data. These studies present detailed insights into the silane decomposition reaction mechanisms and diverse modeling approaches for FBR systems. However, few studies have focused explicitly on devising control strategies for silane pyrolysis in fluidized systems. White et al. (2006) proposed a simplified model that can be easily tuned using experimental data, facilitating control purposes. Their work integrated feedback control theory into steady-state simulations to maintain a constant mass hold-up in the reactor and average product size. Several multiphase gas-solid simulation studies have used computational fluid dynamics tools to examine FBR system dynamics and improve model reliability. These simulations have informed the development of multi-scale modeling approaches that integrate data, such as void fraction, drop pressure, and temperature profiles, into deterministic models. While previous studies, including those by Guenther et al. (2001), Parker (2011), and White et al. (2007), have primarily employed traditional control strategies due to the complexity of the models, other works by Balaji et al. (2010) has demonstrated the potential for more sophisticated control approaches. Du et al. (2014) proposed a multi-scale model structure for silicon production in FBR systems that could be integrated with a control method. Nevertheless, the

control strategies employed in these studies have focused solely on regulating mass hold-up and particle size distribution, overlooking the critical objective of minimizing powder loss to improve process yield. Advanced control strategies, such as model predictive control (MPC), appear promising in addressing this challenge.

This work focuses on developing a predictive modeling framework for particulate polysilicon reactor systems for process control and real-time decision-making applications. Reduced-order models are created for ideal and non-ideal mixed-flow conditions. These models are then utilized as the basis for MPC designs, aiming to precisely regulate particle size distributions and minimize powder loss. The ultimate goal is to enhance the operational efficiency of FBR systems and concurrently reduce production costs associated with solar-grade silicon. The developed reduced-order models encompass a comprehensive integration of reaction mechanisms, population balance, and mass balances for the various components involved in the reaction medium. The subsequent sections of this paper are organized as follows: Section 2 provides a detailed description of the particulate process under consideration. Section 3 thoroughly explores the intricacies of model development and the discretization scheme employed for solving the PBE. Following this, Section 4 establishes the mathematical formulation of the MPC theory. Section 5 is also dedicated to presenting and discussing the outcomes of both open-loop and closed-loop simulations.

2. PROCESS DESCRIPTION

The schematic of the FBR utilized in polysilicon production is illustrated in Fig. 1. The bed commences with an initial preload of silicon seed particles to initiate silicon deposition. A mixture of preheated silane and hydrogen is introduced at the bottom of the reactor to achieve fluidization of the silicon particles. The fluidized bed's temperature is regulated using wall heaters and a preheated inlet gas stream. Upon reaching the designated reaction temperature (650°C), silane's thermal decomposition occurs, leading to solid silicon and hydrogen formation through pyrolysis. The following overall reaction intricately governs this process,

$$\mathrm{SiH_4\,(g)} \longrightarrow \mathrm{Si\,(s)} + 2\,\mathrm{H_2\,(g)}$$

The thermal decomposition of SiH_4 gas forms Si and H_2 through two primary mechanisms. Firstly, silane engages in heterogeneous chemical vapor deposition at the surface of solid silicon, depositing as a crystalline solid. Secondly, silane undergoes homogeneous decomposition, producing a gaseous precursor that can nucleate and generate an amorphous brown powder. A substantial portion of this powder is scavenged by existing silicon particles, subsequently re-crystallizing to contribute to particle growth. Consequently, the silicon seed particles, constituting the product, undergo growth within the reactor and are later extracted from the bottom. The product particles are withdrawn at a regulated rate to maintain the solid hold-up inside the reactor. The remaining fines are exhausted alongside hydrogen gas and unreacted silane at the top exit, diminishing the yield due to powder loss. Minimizing powder loss emerges as a pivotal factor in enhancing the overall yield of the process. Additionally, seed particles are introduced into the reactor to achieve the desired product size distribution.

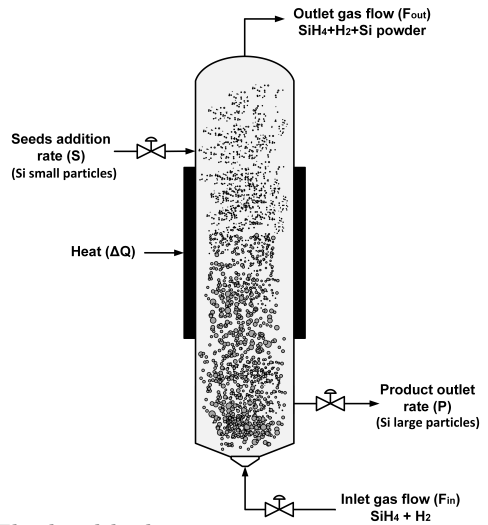

Fig. 1. Fluidized bed reactor.

3. PROCESS MODEL DEVELOPMENT

3.1 Reaction module

Silane undergoes thermal decomposition through two reaction mechanisms. The first involves homogenous decomposition into a gaseous intermediate, which is subsequently scavenged by seed silicon particles. The rate of homogeneous decomposition of silane is expressed as

$$r_{\mathrm{hom}} = 2 \times 10^{13} \exp\left(\frac{-26000}{T}\right) C_{\mathrm{SiH_4}} \tag{1}$$

The homogeneous decomposition generates an intermediate, instigating the nucleation of a new silicon phase (fines). Silicon vapor is assumed to be the gaseous intermediate. The silicon nucleation rate is described by the classical theory of homogeneous nucleation (Abraham (1974))

$$r_{\mathrm{HN}} = N_A \frac{\alpha_c}{\rho} \left(\frac{2\hat{\sigma} m}{\pi}\right)^{1/2} \exp\left(\frac{-4\pi \hat{r}^2 \hat{\sigma} N_A}{3RT}\right) c_{Si}^2 \tag{2}$$

where N_A is Avogadro's number and α_c is the condensation coefficient. The critical radius nuclei $\hat{r}$ is determined by

$$\hat{r} = \frac{2\sigma_{Si}}{\rho_p RT \ln S} \tag{3}$$

where $S = P_{Si}/P_{Si}^0$ is the supersaturation ratio and P_{Si}^0 is the silicon vapor pressure at equilibrium, determined by the following equation (Lai et al. (1986)) when the temperature is below 1685 K,

$$\log(P_{Si}^0) = 7.5341 - 2.3399 \times 10^4/T \tag{4}$$

The specific surface energy ($\hat{\sigma}$) of condensed-phase silicon nuclei is approximated based on the surface tension at the melting temperature (σ_m) (Du et al. (2014)),

$$\hat{\sigma} = \sigma_m \left(\frac{7500 - T}{7500 - T_m}\right)^{1.2} \tag{5}$$

The concentration of silicon vapor is suppressed by diffusion and condensation on large particles and by molecular bombardment of powders. The rate of molecular diffusion

of silicon vapor onto larger particles is expressed by (Friedlander et al. (2000))

$$r_{dl} = \frac{2D_g}{d_p}(C_{Si} - C^0_{Si}) \tag{6}$$

where D_g is the molecular gas diffusion coefficient calculated by

$$D_g = \frac{k_B T}{3\pi\mu d_{pf}} \tag{7}$$

with k_B is the Boltzmann constant, μ is the viscosity of the gas phase, and d_{pf} is the diameter of fine particles. The rate of molecular bombardment of silicon vapor on powder is also determined by

$$r_{df} = \left(\frac{RT}{2M_{si}}\right)^{1/2}(C_{Si} - C^0_{Si}) \tag{8}$$

A fraction of the generated fines due to silicon molecule nucleation is captured by larger particles, thereby contributing to overall particle growth. The rate at which fines are scavenged can be estimated using the following expression,

$$R_{sc} = k_{sc} C_f \tag{9}$$

where C_f denotes the concentration of fines generated by nucleation and k_{sc} is an adjustable proportionality constant. The appropriate value for k_{sc} must be determined by comparing model predictions and experimental data (Balaji et al. (2010)). As indicated in White et al. (2006), the proportionality constant $k_{\mathrm{sc}}\,[m^3/s]$ falls within the range $0 \leq k_{\mathrm{sc}} \leq V_{\mathrm{g}}$.

An alternative reaction pathway involves the heterogeneous decomposition of silane occurring either on the surface of the pre-existing seed silicon particles or onto the fines generated, ultimately resulting in chemical vapor deposition.

$$r_{het} = 2.79 \times 10^8 \exp\left(\frac{-19530}{T}\right) C_{\mathrm{SiH_4}} \tag{10}$$

Therefore, the overall decomposition rate of silane is expressed by

$$R_{total} = r_{het}(A_{tl} + A_{tf}) + r_{hom} V_g \tag{11}$$

where V_g denotes the gas phase volume, calculated as the difference between the total reactor volume (V) and the volume occupied by the solid phase (V_s). The volume of the solid phase is determined by the density of solid silicon, with an assumption of negligible porosity in the solid particles, where $V_s = M_{solid}/\rho$ and M_{solid} and ρ represent the quantity of solid silicon and its density, respectively. Subsequently, A_{tl} denotes the available surface area of the larger particles (seed particles), while A_{tf} pertains to the available surface area of fine particles (powder). The surface area of seed particles (A_{tl}) is assessed using the population balance equation, as elaborated in the subsequent section. Conversely, for the surface area of fines (A_{tf}), an approximation is made by considering the average diameter (d_{pf}) of fine particles found in the literature (Du et al. (2014)).

The increase in silicon particle size within the reactor is facilitated through direct chemical vapor deposition onto the surface of seed particles and the incorporation of fines generated during the reaction. Consequently, the overall deposition rate (Y) on seed particles is a combination of the heterogeneous decomposition rate (r_{het}), the molecular diffusion rate of silicon vapor (r_{dl}), and the scavenging rate (R_{sc}),

$$Y = A_{tl}(r_{het} + r_{dl}) + R_{sc} \tag{12}$$

A portion of the fines produced remains unscavenged by the larger particles. This residual powder is transported out of the reactor alongside hydrogen and silane in the gas phase, increasing the yield loss. The proportion of unrecovered fines, often referred to as powder loss, can be assessed by considering it as a function of both the total deposition rate and the reaction rate of silane,

$$F_f = 1 - \frac{Y}{R_{total}} \tag{13}$$

3.2 Population Balance

A discrete population balance model is employed to predict the particle size distribution achieved during the process. The discretization approach is illustrated in Fig. 2. White et al. (2006) introduced a discrete representation of the population balance equation, streamlining the modeling task. This representation ensures the preservation of conservation laws across all discretization levels, thereby reducing computational costs without additional discretization. Notably, this approach converges to the classical population balance equation when the number of discrete intervals approaches infinity (White et al. (2006)).

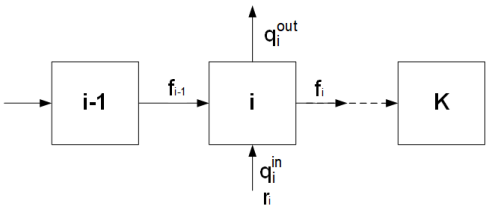

Fig. 2. Discrete size interval network.

The analysis assumes that particles are distributed across K intervals (classes), each characterized by an average number of moles (or mass) per particle. Consequently, each class contains a specific number of particles denoted as N_i, with an average mass m_i. The correlation between the overall mass of the particles and the quantity of particles within each class is expressed as

$$M_i = m_i N_i \quad \forall i = 1, 2, \ldots, K \tag{14}$$

The total available surface area of the particles in a class is defined by

$$A_i = a_i N_i \tag{15}$$

where a_i represents the surface area of a particle within the size class i. Experimental measurements have consistently demonstrated that the shape of silicon particles closely approximates a sphere. Hence, the surface area of a particle with diameter l is calculated by the following expression

$$a_i = 4\pi\left(\frac{l}{2}\right)^2 \tag{16}$$

Particle growth is initiated through deposition onto the particles and a scavenging process, prompting their transition from one size class to the subsequent size category. Consequently, the mass balance for each size class is articulated as follows

$$\frac{dM_i}{dt} = f_{i-1} + f_i + r_i + q_i \tag{17}$$

The conservation equation for the quantity of particles within each class is expressed as

$$\frac{dN_i}{dt} = \frac{q_i}{m_i} - \frac{f_i}{m_i} + \frac{f_{i-1}}{m_i} \tag{18}$$

where $q_i = q_i^{\text{in}} - q_i^{\text{out}}$ represents the total external flow of particles. This quantity is explicitly defined as the difference between the rate of addition of seed particles q_i^{in} within the class i and the particle withdrawal flow q_i^{out}. The rate of mass transfer from the gas phase to the particles within each class is expressed as

$$r_i = Y \frac{A_i}{\sum_i A_i} \quad \forall i = 1, 2, \ldots, K \tag{19}$$

The key parameter connecting the rate of silane decomposition to particle growth in the population balance is the total deposition rate Y. Molar flows of particles occur between consecutive particle size classes. Specifically, the molar flow entering the size class i is denoted as f_{i-1}, whereas f_i represents the molar flow existing in the class. Notably, this study does not consider the effects of agglomeration and attrition. White et al. (2006) proposed an expression linking molar flows between neighboring classes,

$$f_i = r_i \frac{m_{i+1}}{m_{i+1} - m_i} \tag{20}$$

Nevertheless, the final class K requires additional considerations. According to the mass balance illustrated in Eq. 20, this concluding class should not involve particle flow to the subsequent class. Consequently, the mass balance and number balance for class K are defined as

$$\frac{dM_i}{dt} = f_{i-1} + r_i + q_i, \quad \frac{dN_i}{dt} = \frac{q_i}{m_i} + \frac{f_{i-1}}{m_i + 1} \tag{21}$$

The final class K has no mass transfer from the fluid phase to the solid particles. The total mass is the cumulative sum of all masses across all classes

$$M_{\text{total}} = \sum_{i=1}^{K} M_i \tag{22}$$

The comprehensive mass balance equation for the solid phase is expressed as follows

$$\frac{dM_{\text{total}}}{dt} = Y + S - P \tag{23}$$

where S is the seed addition rate, Y is the total deposition rate, and P is the product withdrawal rate. Sustaining a consistent level in the solid bed is crucial for ensuring stable fluidization conditions during operation. This goal can be achieved by controlling the total mass hold-up of silicon particles within the reactor. The regulation of the total mass hold-up is facilitated by manipulating the flow of product withdrawal. Therefore, an inventory control strategy for the silicon mass hold-up (White et al. (2006)) can be defined as

$$\frac{dM_{\text{total}}}{dt} = K_m (M_{\text{total}} - M^*) \tag{24}$$

where K_m is a proportional gain constant and M^* is the desired mass hold-up. Consequently, the expression for product withdrawal can be formulated as

$$P = S + Y + K_m (M_{\text{total}} - M^*) \tag{25}$$

The proposed control strategy effectively regulates the mass hold-up in the system, taking into account the product withdrawal rate. The average particle size is determined by employing the weighted average approach, derived from the particle size distribution,

$$d_p = \frac{1}{\sum_i w_i / d_{pi}} \tag{26}$$

where w_i represents the fraction (weight) of i-th class in the distribution, and d_{pi} denotes the particle diameter.

3.3 Flow regimes and mass balances

Well-mixed flow regime: The fluid dynamics and gas-solid interactions within the fluidized reactor present inherent complexities. Nonetheless, under certain operational conditions, the system's behavior can be reasonably approximated as that of an ideally well-mixed reactor. This approximation becomes feasible in fluidized beds only when bubble formation is effectively suppressed while ensuring robust solid-gas mixing (Lai et al. (1986)). Assuming well-mixed conditions for both the solid and gas phases within the reactor, the mass balances for the gas phase are expressed as follows

$$\begin{aligned}
\frac{dM_{\text{SiH}_4}}{dt} &= F^{in} C^{in}_{\text{SiH}_4} - F^{out} C^{out}_{\text{SiH}_4} \\
&\quad -(r_{hom} V_g + r_{het}(A_{tl} + A_{tf})) \\
\frac{dM_{\text{H}_2}}{dt} &= F^{in} C^{in}_{\text{H}_2} - F^{out} C^{out}_{\text{H}_2} \\
&\quad +2(r_{hom} V_g + r_{het}(A_{tl} + A_{tf})) \\
\frac{dM_{\text{Si}}}{dt} &= (r_{hom} - r_{hn}) V_g - r_{dl}(A_{tl} + A_{tf}) \\
\frac{dM_f}{dt} &= r_{hn} V_g - R_{sc} - F^{out} C^{out}_f + r_{het} A_{tf}
\end{aligned} \tag{27}$$

This particle growth system involves several distinct time scales. The silane decomposition reaction is almost instantaneous and reaches completion over a few centimeters at the reactor's entrance (Caussat et al. (1995)). The flow and mixing regimes stabilize into steady-state conditions within a few seconds of operation. Additionally, contingent upon the inlet conditions, the temperature can attain a steady state after a few minutes (Balaji et al. (2010)). In contrast, particle size growth proceeds at a markedly slower pace, with changes in the particle size distribution taking place over days (Du et al. (2014)). Consequently, Eqs. 27 can be solved under pseudo-steady state conditions.

Plug flow regime: The assumption of an ideal mixed flow reactor can only be applied to describe system dynamics under particular conditions. However, experiments indicate that the process yield may exhibit variability based on the prevailing process conditions, stem from concentration gradients within the fluid phase, or inconsistent operational parameters (Balaji et al. (2010)). Notably, the existing equations within the CSTR framework fail to account for the gas phase concentration gradients across the reactor. Hence, to offer a more encompassing representation of the system's dynamics, the present study proposes to model the gas phase as a plug-flow reactor under pseudo-steady state conditions. This adjustment aims to capture the nuanced dynamics of the gas phase within the reactor, which are essential for a comprehensive understanding of the system,

$$\begin{aligned}\frac{dM_{\mathrm{SiH_4}}}{dx} &= -r_{hom}V_g - r_{het}(A_{tl}+A_{tf})\\ \frac{dM_{\mathrm{H_2}}}{dx} &= -2\big(r_{hom}V_g + r_{het}(A_{tl}+A_{tf})\big)\\ \frac{dM_{\mathrm{Si}}}{dx} &= (r_{hom}-r_{hn})V_g - r_{dl}(A_{tl}+A_{tf})\\ \frac{dM_f}{dx} &= r_{hn}V_g - R_{sc} + (r_{dl}+r_{het})A_{tf}\end{aligned} \tag{28}$$

In this case, both the silane decomposition rate and the total deposition rate exhibit dependence on the reactor height. Integrating these parameters into the discrete population balance scheme necessitates the calculation of their respective average values, as expressed by

$$\begin{aligned}R_{total} &= \frac{1}{h}\int \big(r_{het}(x)(A_{tl}+A_{tf}) + r_{hom}(x)V_g\big)\,dx\\ Y &= \frac{1}{h}\int \Big(A_{tl}\big(r_{het}(x)+r_{dl}(x)\big) + R_{sc}(x)\Big)\,dx\end{aligned} \tag{29}$$

where h is the reactor height.

4. NONLINEAR MODEL PREDICTIVE CONTROL

Model predictive control (MPC) is an advanced control strategy capable of predicting future process states to estimate optimal control actions within the constraints of the process (Rawlings et al. (2017)). MPC consists of three integral components: an objective function, a process model, and a dynamic optimizer. Leveraging the process model, MPC predicts the system's state response by considering the inherent physical phenomena. Subsequently, real-time optimization comes into play, determining the optimal control action by resolving a dynamic optimization problem,

$$\min_u \; J\big(x(t),u(t)\big) = \int_t^{t+T_p} F\big(x(\tau),u(\tau)\big)\,d\tau \tag{30}$$

subject to the nonlinear process model

$$\dot{x}(t) = f\big(x(t),u(t)\big), \quad x(0)=x_0 \tag{31}$$

and input and state constraints

$$\begin{aligned} u(\tau) &\in \mathcal{U} \quad \forall\tau\in[t,t+T_c]\\ x(\tau) &\in \mathcal{X} \quad \forall\tau\in[t,t+T_p]\\ C(x,u,t) &= 0\\ D(x,u,t) &\le 0\end{aligned} \tag{32}$$

where

$$\begin{aligned}\mathcal{U} &:= \{u\in R^m \,|\, u_{\min}\le u\le u_{\max}\}\\ \mathcal{X} &:= \{x\in R^n \,|\, x_{\min}\le x\le x_{\max}\}\end{aligned} \tag{33}$$

where $x(t)\in R^n$ and $u(t)\in R^m$ represent the state and input vectors, respectively. The vectors $u^{\max}$ and $u^{\min}$ denote the upper and lower bounds for the manipulated inputs, while $x^{\max}$ and $x^{\min}$ specify the upper and lower bounds for the state vector. T_p and T_c represent the prediction and control horizons, respectively, where $T_c \le T_p$. The functions C and D encompass nonlinear vector functions that correspond to the equality and inequality constraints inherent in the system. The cost function J under consideration is quadratic,

$$\begin{aligned}F\big(x(\tau),u(\tau)\big) &= (x-x_s)^T Q(x-x_s)\\ &\quad +(u-u_s)^T W(u-u_s)\end{aligned} \tag{34}$$

where x_s and u_s represent the desired reference vector values (targets) for the system state and manipulated inputs, respectively. These reference values may be constant or time-varying. The positive definite weight matrices $Q\in R^{n\times n}$ and $W\in R^{m\times m}$ are adjusted to impose penalties on the errors in state regulation and manipulated variables within the objective function (Pourkargar et al. (2017)). The system model utilized to predict the response is initialized based on the actual system state, which can be either directly measured or estimated. Solving the optimization problem yields the optimal sequence of control actions $u^*(\cdot,x(t)) : [t,t+T_p]\to\mathcal{U}$ over the prediction horizon $[t,t+T_p]$. Following this, the computed vector of manipulated variables during the prediction horizon is applied, with only the first control input of the sequence being implemented at time t. Subsequently, the optimization process recommences for the next sampling period.

5. SIMULATION RESULTS AND DISCUSSIONS

Table 1 outlines the simulation parameters employed in this study. In our investigation, we utilized 20 size intervals. The average particle size within each interval is documented in a prior study by Du et al. (2014). The associated initial bed distribution and seed size distribution are depicted in Fig. 3.

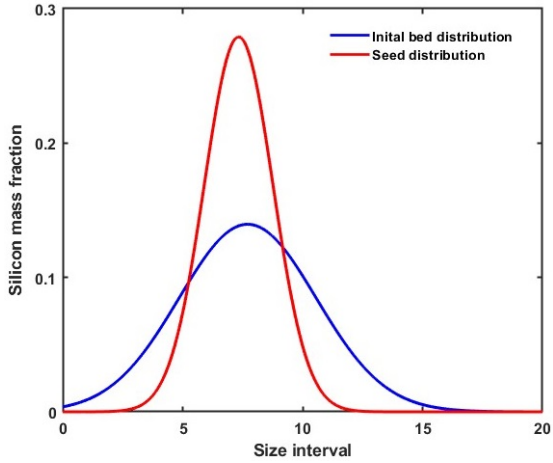

Fig. 3. Particle size distributions used for the simulations.

Table 1. Initial Conditions.

Parameter	Value	Symbol
Reactor height	7 m	h
Reactor diameter	0.5 m	D
Inlet gas velocity	0.55 m/s	v_{in}
Inlet Concentration - Silane	6.5 mol/m^3	$C^{\mathrm{in}}_{\mathrm{SiH_4}}$
Inlet Concentration - Hydrogen	1.6 mol/m^3	$C^{\mathrm{in}}_{\mathrm{H_2}}$
Inlet Concentration - Silicon Powder	0.001 mol/m^3	$C^{\mathrm{in}}_{\mathrm{Si}}$
Scavenging factor	0.03 m^3/s	k_{sc}
Fine diameter	$0.3\times10^{-6}m$	d_{f}
Seed addition rate	0.001 mol/s	S
Initial Solid bed	350 kg	M
Mass hold-up	450 kg	M^*
Reactor Temperature	850 K	T

5.1 Open-loop simulations

Fig. 4 presents the open-loop particle growth dynamics, showcasing the evolution of the critical process properties over time. According to the simulation results, the particle growth dynamics reach steady state conditions after 125

hours. Fig. 4a displays the average particle sizes predicted by both modeling approaches. While minimal differences exist in the steady-state values obtained from both models, a notable disparity emerges in the transient region. This mismatch is associated with the different deposition rates calculated in each modeling approach. Precisely, the well-mixed flow regime approach attains steady-state conditions more rapidly due to a higher initial deposition rate. Conversely, the plug flow regime approach yields a lower deposition rate due to incorporating concentration gradients in the calculations.

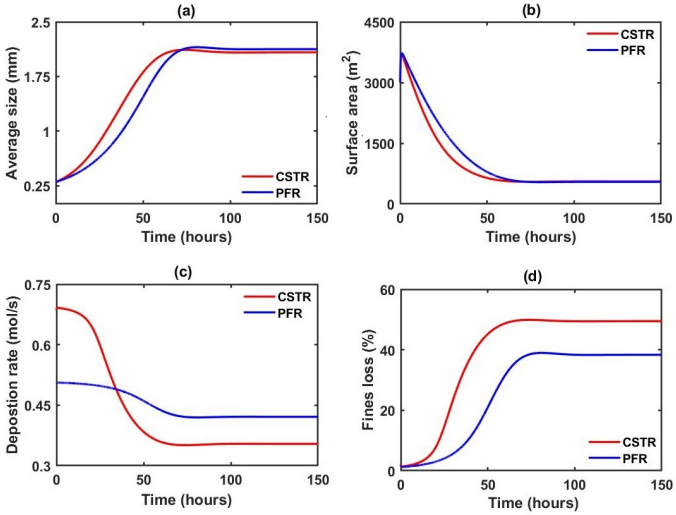

Fig. 4. Open-loop system dynamics for (a) average particle size, (b) available surface area, (c) total deposition rate, and (d) powder loss.

The change in the particle size distribution due to the particle growth reduces the available surface area for chemical vapor deposition onto the seed particles. A substantial reduction in the available surface area of seed particles is observed in Fig. 4b. This decrease in surface area diminishes the effectiveness of chemical vapor deposition, stemming from the heterogeneous decomposition of silane and the molecular diffusion of silicon vapor to facilitate particle growth. Consequently, there is a notable reduction in the overall deposition rate (Fig. 4c).

The projected powder loss for each model is presented in Fig. 4d. Both models predict a powder loss exceeding 40% of the generated powder under steady-state conditions. However, the well-mixed flow approach predicts a higher power loss. Minimizing powder loss is imperative to enhance the process yield. Several factors contribute to increased powder loss, including elevated temperatures, which promote fines formation due to the higher activation energy of the homogeneous decomposition reaction compared to the heterogeneous mechanism. Additionally, higher inlet gas velocities can carry more fine particles in the gas phase at the top of the FBR system. Consequently, operating at high temperatures or increased inlet gas velocities leads to a diminished process yield.

Generally, at low temperatures and low gas flow rates (near the minimum fluidization velocity), the predictions of these two models align closely. However, achieving the ideal well-mixed condition, especially at minimum fluidization conditions, is challenging. Furthermore, the well-mixed flow regime modeling approach oversimplifies the system by neglecting concentration and temperature gradients in its calculations. In contrast, the plug flow regime approach offers a more accurate system representation, making it suitable for control and decision-making.

5.2 Closed-loop Simulations

The prediction and control horizons are set to $N_p = N_c = 10$ sampling, with a sampling time of $\Delta = 5$ hours for each MPC iteration. Consequently, the prediction horizon for solving the optimal control problem at each sampling instance is determined as $T_p = T_c = 50$ hours. It is assumed that all states are accessible at the designated sampling times. The control objective is stabilizing the system at the steady-state condition detailed in Table 2.

Table 2. Steady State Values.

Parameter	Value	Symbol
Mass hold-up	450 kg	x_1^{SS}
Average Particle size	2.10 mm	x_2^{SS}
Seed addition rate	0.001 mol/s	u_1^{SS}
Inlet gas velocity	0.55 m/s	u_2^{SS}

The interior-point optimization algorithm (IPOPT) is employed to address the nonlinear constrained dynamic optimization problem at each sampling time (Biegler (2010)). Given the nonconvex nature of the optimization problem, the assurance of a global minimum value is not guaranteed. Weight matrices are utilized to balance the importance of each state and input variable in the cost function. However, in this context, mass hold-up and particle size distribution are deemed equally significant, as are the manipulated inputs. Consequently, identity matrices are chosen for both weight matrices Q and W. The controlled variables encompass the product's mass hold-up and particle size distribution, crucial for ensuring the system's proper operation. However, the non-self-regulating nature of the mass hold-up dynamic necessitates constraints to avoid convergence to different steady states or instability when determining associated flow rates. Eq. 25 is integrated into the MPC controller as a nonlinear constraint to regulate the product withdrawal rate.

The second controlled variable is the particle size distribution of the product. The physicochemical and mechanical properties of particulate system products hinge strongly on the corresponding particle size distribution characteristics. Manipulating the particle size distribution is thus fundamental for controlling product quality. The product size distribution depends on the seed added to the reactor and the ratio between the seed mass and the total mass. Hence, the seed addition rate can be used as a manipulated variable. The seed addition rate influences the product size distribution, while the inlet gas velocity regulates the deposition rate by controlling the amount of silane in the reactor. Additionally, these manipulations can be considered to minimize power loss in the FBR system. Consequently, the seed addition rate and the inlet gas flow rate are manipulated inputs for the MPC controller, constrained within $\pm 50\%$ of their steady-state values outlined in Table 2.

Fig. 5 illustrates the closed-loop simulation employing the plug flow regime model approach. State variables and

inputs are presented in normalized deviation form. Figs. 5a and 5b depict the seed addition rate and the inlet gas velocity gradually converging to their steady-state values. After 50 hours, the control actions reach a steady-state condition, remaining constant.

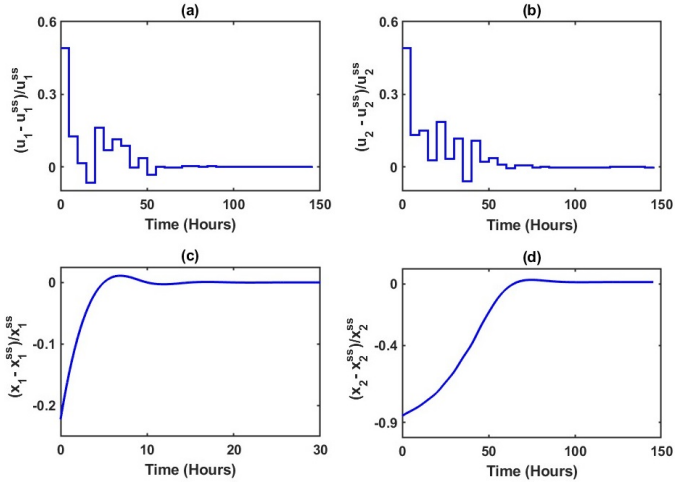

Fig. 5. Closed-loop system dynamics: (a) seed addition rate, (b) inlet gas velocity, (c) mass hold-up, (d) average particle size.

Fig. 5c presents the dynamic response of the mass hold-up, revealing a faster dynamic response compared to the average particle size illustrated in Fig. 5d. A slight overshoot is observed before the system attains its steady-state value. This overshooting behavior results from the control strategy outlined in Eq. 25, integrated with MPC. Turning attention to Fig. 5d, the transient response in the particle size distribution is evident, requiring a more extended period to achieve a steady-state condition. The sluggish evolution of the average particle size can be attributed to the gradual dynamics inherent in the particle growth process. In summary, both state variables exhibit convergence with smooth trajectories, indicating the successful stabilization of the system at their respective steady-state values.

6. CONCLUSION

This work presents a control-oriented predictive model for polysilicon production in FBR systems. The developed model uniquely integrates concentration gradients to characterize silane decomposition along the reactor and employs population balance principles to anticipate particle growth. The successful integration of nonlinear MPC with the proposed model is demonstrated through simulation results. These findings showcase the MPC controller's effectiveness in regulating mass hold-up and controlling particle size distribution in the final product. The introduced predictive modeling and control framework holds promise for advancing control strategies used in particulate systems operation, thereby contributing to the optimization of silicon production within fluidized systems. Our future investigations emphasize controlling reactor temperature and enhancing the scavenging rate to minimize powder loss, providing avenues for further refinement and improvement in the overall process.

REFERENCES

Abraham, F.F. (1974). *Homogeneous nucleation theory*, volume 263. Elsevier.

Balaji, S., Du, J., White, C., and Ydstie, B.E. (2010). Multi-scale modeling and control of fluidized beds for the production of solar grade silicon. *Powder Technology*, 199(1), 23–31.

Biegler, L.T. (2010). *Nonlinear programming: Concepts, algorithms, and applications to chemical processes*. SIAM.

Cadoret, L., Reuge, N., Pannala, S., Syamlal, M., Coufort, C., and Caussat, B. (2007). Silicon CVD on powders in fluidized bed: Experimental and multifluid Eulerian modeling study. *Surface and Coatings Technology*, 201(22-23), 8919–8923.

Caussat, B., Hemati, M., and Couderc, J. (1995). Silicon deposition from silane or disilane in a fluidized bed—Part II: Theoretical analysis and modeling. *Chemical engineering science*, 50(22), 3625–3635.

Du, J., Dutta, S., and Ydstie, B.E. (2014). Modeling and control of solar-grade silicon production in a fluidized bed reactor. *AIChE Journal*, 60(5), 1740–1751.

Friedlander, S.K. et al. (2000). *Smoke, dust, and haze*, volume 198. Oxford university press New York.

Guenther, C., O'Brien, T., and Syamlal, M. (2001). A numerical model of silane pyrolysis in a gas-solids fluidized bed. In *Proceedings of the International Conference on Multiphase Flow*. Citeseer.

Kunii, D. and Levenspiel, O. (1968). Bubbling bed model. model for flow of gas through a fluidized bed. *Industrial & Engineering Chemistry Fundamentals*, 7(3), 446–452.

Lai, S., Ramachandran, P., et al. (1986). Chemical vapor deposition and homogeneous nucleation in fluidized bed reactors: Silicon from silane. *Chemical Engineering Science*, 41(4), 633–641.

Parker, J.M. (2011). Validation of CFD model for polysilicon deposition and production of silicon fines in a silane deposition FBR. *International Journal of Chemical Reactor Engineering*, 9(1).

Pourkargar, D.B., Almansoori, A., and Daoutidis, P. (2017). Impact of decomposition on distributed model predictive control: A process network case study. *Industrial & Engineering Chemistry Research*, 56(34), 9606–9616.

Ramkrishna, D. (2000). *Population balances: Theory and applications to particulate systems in engineering*. Elsevier.

Rawlings, J.B., Mayne, D.Q., and Diehl, M. (2017). *Model predictive control: Theory, computation, and design*. Nob Hill Publishing Madison, WI, 2 edition.

Tejero-Ezpeleta, M.P., Buchholz, S., and Mleczko, L. (2004). Optimization of reaction conditions in a fluidized-bed for silane pyrolysis. *The Canadian Journal of Chemical Engineering*, 82(3), 520–529.

White, C.M., Ege, P., and Ydstie, B.E. (2006). Size distribution modeling for fluidized bed solar-grade silicon production. *Powder technology*, 163(1-2), 51–58.

White, C.M., Zeininger, G., Ege, P., and Ydstie, B.E. (2007). Multi-scale modeling and constrained sensitivity analysis of particulate CVD systems. *Chemical Vapor Deposition*, 13(9), 507.